ISSN 0915-633X

NATIONAL INSTITUTE FOR FUSION SCIENCE

Current-profile Flattening and Hot Core Shift due to the Nonlinear Development of Resistive Kink Mode

K. Watanabe, T. Sato and Y. Nakayama

(Received - Sep. 20, 1994)

NIFS-311 Oct. 1994

RESEARCH REPORT
NIFS Series

NAGOYA, JAPAN

Current-profile Flattening and Hot Core Shift due to the Nonlinear Development of Resistive Kink Mode

Kunihiko Watanabe and Tetsuya Sato

Theory and Computer Simulation Center

National Institute for Fusion Science, Nagoya 464-01, Japan

Yuichiro Nakayama

Canon Systems Globalization, Inc., Santa Clara 95054, U.S.A.

Keywords

tokamak, current profile, computer simulation, magnetohydrodynamics, magnetic reconnection

Abstract

A new and interesting phenomenon showing that the toroidal current profile for the n=0 mode, which at first exhibits a peak due to ohmic heating and later flattens around the magnetic axis, is obtained through a compressible resistive MHD simulation in a fully 3-D toroidal geometry. We conclude through a detailed analysis that the current flattening is caused by the strong excitation of a nonlinear resistive kink mode. The time-scale of the current profile flattening is of the order of the MHD time-scale. When the current profile is largely flattened, the plasma dynamic pressure due to the strongly excited kink mode pushes the hot core plasma in the radial kink flow direction and the hot core starts deviating from the magnetic surface because of the plasma compressibility and the dynamic pressure. Since the flattening of a current profile weakens the shear effect of the poloidal magnetic field in the $q < 1$ region where the resistive kink mode is growing, the poloidal magnetic field reconnection is driven by the strong kink flow and leads to complete destruction of the magnetic surface within the q=1 rational surface (minor disruption), and the poloidal magnetic field configuration recovers to an axi-symmetric profile. The effect of the thermal conduction on the evolution of such a process is also discussed.

1. INTRODUCTION

The MHD stability problem such as the resistive/ideal kink mode and the tearing mode as well as the minor/major disruption process has long been a subject of vital interest. In such MHD activities, the toroidal current profile plays an essential role. The important point is to note that the current profile, realistically, does not remain static in the actual tokamak plasma. Nevertheless, most of the studies have been made under a given (i.e. static) current profile, except for simulation researches such as Aydemir's simulation studies on the tokamak sawtooth phenomena [1,2]. In fact, the analytical method often fails to investigate the MHD activities in the tokamak plasma under the time evolving circumstances. In other words, the dynamic behavior of the current profile and its dynamic effects on the MHD activities call for a thorough investigation, which can be best performed by means of an elaborate computer simulation.

Our present study aims to clarify the process of dynamic response of the current profile change on the MHD stability in a tokamak plasma within the classical MHD framework. To fulfill this aim, we execute a three-dimensional compressible resistive MHD simulation for a torus geometry, taking into account a thermal conduction effect in the direction parallel to the magnetic field.

2. SIMULATION MODEL AND RESULTS

The basic equations are

$$\frac{\partial \rho}{\partial t} + \nabla \cdot (\rho \vec{v}) = 0, \tag{1}$$

$$\rho \frac{d \vec{v}}{d t} = \vec{j} \times \vec{B} - \nabla p, \tag{2}$$

$$\frac{\partial \vec{B}}{\partial t} = \nabla \times (\vec{v} \times \vec{B}) - \nabla \times (\vec{j}/S), \tag{3}$$

$$\frac{\partial p}{\partial t} + \nabla \cdot (p \vec{v}) = (\gamma - 1)(-p \nabla \cdot \vec{v} + \vec{j}^2/S) + \kappa \Delta_{//} T, \tag{4}$$

where the magnetic Reynolds number S is classical and proportional to the 3/2 power of the temperature. The thermal conduction effect, $\kappa\Delta_{//}T$, is introduced only in the direction parallel to the magnetic field, where κ is constant. Here, it should be noted that the time-scale of the thermal conduction effect is assumed to be of the same order as the MHD time-scale in this study.

The tokamak device is modelled by a torus surrounded by a conducting wall with a square cross section as shown in Fig. 1, where the cylindrical coordinates (R, θ, Z) are adopted ; R is the major radius, θ the toroidal angle, and Z the vertical axis. We solve the above MHD equations using a high precision code recently developed by us which advances the physical quantities in time using the fourth order Runge-Kutta-Gill method and makes a spatial differentiation using the fourth order centered-difference method [3,4]. The simulation is performed through the following two stages :

First, in order to obtain the initial equilibrium configuration without resistivity, we solve the Grad-Shafranov equation under the above geometry where the toroidal β and the aspect ratio are taken to be 0.1% and 3, respectively. The on-axis q value is set to be 1.03, and thus, the obtained equilibrium state is confirmed to be stable for the n=1 mode by running the simulation code.

Next, we impose a very small plasma flow disturbance of n=1 mode as well as the resistivity upon the initial equilibrium configuration, and start simulation. Here, the initial on-axis S value is set to be 40000 and its distribution is known from the temperature distribution.

In Fig. 2, shown are the toroidal current distributions of the n=0 mode against the minor radius at a poloidal cross section for t=0, t=415 τ_{pA}, t=447 τ_{pA} and 480 τ_{pA}, where the magnetic axis corresponds to r = 0 ($\tau_{pA} = a/V_{pA} = R_0/V_{tA}$ denotes the poloidal Alfven transit time). As can be seen in the figure, the toroidal current undergoes peaking around the axis till t=415 τ_{pA}, because the resistivity distribution changes subject to

spatially dependent ohmic heating and the quantity $\vec{j}/S$ tends to become curl-free. The toroidal current profile, however, becomes flattened quickly during a short period of 65 τ_{pA} from t=415 τ_{pA} till 480 τ_{pA}. The flattened region extends almost over the q = 1 magnetic rational surface.

Fig. 3 shows the time development of the magnetic field energies of the n=1 mode (linear mode) and the n=2 mode (nonlinear mode). Since the initial q value is greater than 1 in the whole region, both the magnetic field energy and the kinetic energy of the superposed plasma flow disturbance suffers damping at first. As the ohmic heating changes the distribution of the plasma temperature, and hence, the resistivity, current peak develops around the plasma axis and this leads to reduction of the q value. At $t = 81\tau_{pA}$, the on-axis q value falls below 1. Then, the m=1/n=1 resistive kink mode becomes unstable and the magnetic field and plasma flow of n=1 mode start growing around the axis. As the q value decreases further, the excited magnetic field intensity of n=1 mode, as well as the plasma flow, becomes larger and larger. It should be noted here that the q value is defined in the present work as the ratio of the number of the toroidal rotation to that of the poloidal rotation around the initial magnetic axis by tracing the magnetic field line along the toroidal direction. The on-axis q value becomes smallest at t=415 τ_{pA} due to current peaking, so that the magnetic field and the plasma flow have large enough magnitude by this time. At t=480 τ_{pA}, a nonlinearly excited mode (n = 2 mode) is also grown roughly up to the amplitude of the most unstable mode (n=1), thus suggesting that the n=0 mode must also have been excited to a substantial amplitude.

In order to confirm that the excited unstable mode shown in Fig. 3 is the resistive kink mode, we made several simulations with different S numbers in which the on-axis q value is fixed to be 0.85 initially. The linear growth rates obtained in these simulations are shown in Fig. 4. In this figure, the theoretical growth rate of the resistive kink mode [5], being proportional to $S^{-1/3}$, is indicated by the solid line. The observed growth rates

show a good agreement with the $S^{-1/3}$ curve, hence, it can be confirmed that the excited mode in these simulations is the resistive kink mode, not the tearing mode whose growth rate is proportional to $S^{-3/5}$. The detailed features of a rapid change in the current profile can be found in Fig. 5 by looking into the evolutions of the equi-contours of the toroidal current of the n=0 mode(upper panels), the magnetic field lines mapped on a poloidal plane(middle panels), and the equi-contours of the temperature(lower panels) at the same moments as those adopted in Fig. 2, namely, at t=0, t=415 τ_{pA}, t=447 τ_{pA} and 480 τ_{pA}.

It can be surely confirmed that the toroidal current which showed peaking at t=415 τ_{pA} becomes flattened at t=480 τ_{pA}. Through this process, no apparent difference is observed in the magnetic surface structure. It is interesting to observe that, at t = 415 τ_{pA}, the temperature axis still stays at its initial position (Fig. 5-(a) and (b)), but at t=480 τ_{pA}, the temperature axis has substantially shifted, although the magnetic axis remains almost at the same position during the period (Fig. 5-(c) and (d)).

This deviation between the magnetic axis and the temperature axis results from the following fact : The strong kink flow, which directs from the center of the axis to the right-side and flows back along the magnetic surface to the left-side to merge into the central flow, pushes the plasma towards the right-side. During this process a dynamic equilibrium is kept where the magnetic pressure is almost in balance with the plasma dynamic pressure, since the plasma static pressure is small in this case. In order to confirm the role of the dynamic pressure causing such a deviation, we executed a linearized simulation run in which the feedback effect of the plasma dynamic flow on the plasma total pressure is discarded. Then, no such a deviation is observed at all. Thus, we conclude that the dynamic plasma pressure surely gives rise to the deviation between the magnetic surface and the temperature equi-contour.

When the toroidal current profile becomes flattened, it is expected that the shear effect of the poloidal magnetic field be lost and that the magnetic surface be destroyed.

In fact, right after the current profile flattening, the plasma kink flow pushed the poloidal magnetic field lines towards the q=1 surface to start triggering driven reconnection [6] from the central part of the plasma at t = 493 τ_{pA}. The flux reconnected by driven reconnection expands radially from the central part and eventually reaches to the q=1 surface. Thus, the whole magnetic flux within the q=1 surface is completely mixed up at the time t = 504 τ_{pA}. In the final stage of this driven reconnection process the magnetic structure returns to the axi-symmetric one (at t = 513 τ_{pA}), as shown in Fig. 6-(a) through (c), respectively.

It should be noticed again that the time span of the last two panels in Fig. 5 in which the current profile becomes flattened is 65 τ_{pA}, and the time span of the first and last two panels in Fig. 6 is only 20 τ_{pA} during which the driven reconnection process is completed. In this respect, it should be noted also that the time span of the former two panels in Fig. 5 during which the q value suffers a substantial resistive change is as long as 415 τ_{pA}. Therefore, it is concluded that the condition for current profile flattening and magnetic surface disruption is made up in the MHD time-scale rather than the resistive one.

3. DISCUSSION

From the simulation results shown here, the toroidal current profile starts being flattened in accordance with the manner that the equi-temperature contours deviate from the magnetic surface. Thus, a question naturally occurs : Is there any correlation between them ? In order to examine whether or not there is any physical necessity in this coincidence, we have made an artificially controlled simulation for $t > 407\tau_{pA}$ in which the magnitudes of the n=0 component of all physical quantities are fixed to those values at t=407 τ_{pA} when the temperature axis remains yet in coincidence with the magnetic axis and the current profile remains peaked. The results at (a) t=447 τ_{pA}, (b) t=480 τ_{pA}, (c) t=493 τ_{pA}, and t=504 τ_{pA} are shown in Fig. 7 which , respectively, correspond to (c) and

(d) in Fig. 5 and (a) and (b) in Fig. 6. No current profile flattening occurs, and hence, no destruction of the magnetic surface is observed, although the equi-temperature contours deviate much from the magnetic surface as was observed in the previous original run.

This fact indicates that the current profile flattening and resultant disruption of the magnetic surface evidently result from strong nonlinear excitation of the resistive kink mode, not from the deviation between the equi-contours of the temperature and magnetic surface .

However, a pertinent question may be raised on the influence of parallel thermal conduction on the current profile flattening. We have thus made a simulation in which the thermal conduction effect is removed completely. The magnetic surface and the equi-contours of the toroidal current and temperature at t = 366 τ_{pA}, 407 τ_{pA}, 451 τ_{pA} and 459 τ_{pA} are shown in Fig. 8. One can easily find that the current profile flattening and resultant disruption do occur in a similar way except that the evolution occurs slightly earlier, say, about 40 τ_{pA} earlier, than that of the case when the thermal conduction effect is taken into account. This indicates that the thermal conduction plays an active role in impeding the evolution and delaying the onset time for the slide-away of the hot core from the central part. Thus, it is conjectured that the transition from the slow ramp-up phase to the fast crash would be very sharp when the parallel thermal conduction is much faster than the MHD behavior.

This impeding effect of the thermal conduction can be explained in the following way. The spatial distribution of the magnetic Reynolds number, S, which is proportional to the 3/2 powers of the temperature, shows a similar dependence to that of the temperature. Therefore, as long as the magnetic surface coincides with the equi-temperature contour, namely, until t = 415 τ_{pA}, the S value is uniform along the same magnetic surface. Once a current profile is flattened in the central part by the nonlinear evolution of the kink mode, however, the quantity $\vec{j}/S$ deviates from the curl-free condition. This is because

the evolution of $\vec{j}$ is primarily governed by the MHD activity, while the evolution of S is highly dependent on the thermal conduction. It is likely therefore that the nonlinear current profile flattening is impeded by the parallel thermal conduction.

Regarding the magnetic surface disruption, it should be remarked that, in a compressible plasma, the time-scale of the driven magnetic reconnection process is weakly dependent on the resistivity, but strongly dependent on the magnitude of the driving plasma flow [7]. Therefore, it is conjectured that the time-scale of the destruction of the magnetic structure within the q=1 rational surface be controlled by the kink flow, not by the resistivity.

It is important to note that the nonlinearly driven reconnection process and the resultant magnetic island formation appear and rapidly grow after t=480 τ_{pA} in the original case. Detailed magnetic field line plots are shown in Fig. 9. Before the time t=480 τ_{pA}, this kind of global reconnection has not been observed, but a gentle resonant reconnection at q=1 surface appears and gradually grows after the on-axis q value becomes below 1. Note that the nonlinear driven reconnection point is located on the opposite side of the q=1 resonant reconnection point in the radial direction with respect to the magnetic axis. In Fig. 9, it is interesting to find that the q=1 resonant reconnection is activated as soon as driven reconnection invades into the magnetic island of the resonant type reconnection at q=1 surface. The magnetic field line plots and the plasma flow at t=505.1 τ_{pA} are indicated in Fig. 10. It is clearly seen that the q=1 resonant reconnection is strongly driven by the plasma flow which goes back around the original magnetic axis to merge with each other on the left-side, while the reconnection inside the q=1 surface is driven by the central main kink flow which directs to the right-side.

Finally, it should be emphasized that the current profile flattening is not the effect of reconnection, but the cause of reconnection. This gives a marked contrast to the conventional Kadomtsev sawtooth model.

4. SUMMARY

The toroidal current profile flattening phenomenon is found by means of a full-torus, compressible, resistive MHD simulation. In this phenomenon, the strong excitation of the n=0 mode through the nonlinear (quasi-linear) coupling of the n=1 resistive kink mode plays an essential role. Simultaneously, there arises a shift of the hot plasma core from the magnetic surface as a result of the strong kink plasma flow that pushes the plasma towards the wall, keeping a dynamic equilibrium. This hot core slide is boosted by the current profile flattening and resulting magnetic flux mixing in the $q < 1$ region due to the excitation of driven reconnection. This can account for the fast crash of a sawtooth phenomenon.

The thermal conduction prevents the deviation from the magnetic surface, thus suppressing the current profile flattening. Nevertheless, the strongly excited nonlinear mode eventually overcomes this effect and leads to eventual current profile flattening and ensuing magnetic surface disruption. The time-scale of the current profile flattening is determined by the time-scale of the mode coupling which is a few tens of τ_{pA}.

In the present study, we employed the parallel thermal conductivity of the order of the MHD time-scale or smaller, because otherwise the type of the equation changes from the hyperbolic to elliptic and the MHD behavior cannot be simulated in a precise manner. In the case when the electron temperature is much higher than the ion temperature, the parallel thermal conduction may play a more active role. However, when the ion temperature is the same order as the electron one, then, the thermal conduction effect may become smaller and the transition may become milder. In other words, the transition would become sharper as the thermal conduction becomes larger. Nevertheless, our simulation study indicates that the current profile flattening due to the nonlinear excitation of the kink mode plays a crucial role in the tokamak MHD activities.

ACKNOWLEDGEMENTS

The authors are grateful for stimulating discussions with R. Horiuchi, T. Hayashi, A. Bhattacharjee, and B. Dasgupta. The authors are also thankful to M. Azumi for his valuable discussions and advises. This simulation research is performed by using the Advanced Computing System for Complexity Simulation at NIFS. The work is supported by Grants-in-Aid of the Ministry of Education, Science, and Culture in Japan (No. 06044238 and No. 05836038).

REFERENCES

[1] Aydemir, A. Y., Wiley, J. C., Ross, D. W., Phys. Fluids, **B1**, (1989) 774.

[2] Aydemir, A. Y., Phys. Fluids, **B2**, (1990) 2135.

[3] Horiuchi, R., Sato, T., Phys. Fluids, **B1**, (1989) 581.

[4] Watanabe, K., Sato, T., J. Geophys. Res., **95**, (1990) 75.

[5] Coppi, B., Galvao, R., Pellat, R., Rosenbluth, M., Rutherford, P., Fiz. Plazmy, **2**, (1976) 961 ; Sov. J. Plasma Phys. **2**, (1976) 553.

[6] Sato, T., Horiuchi, R., Kusano, K., Phys. Fluids, **B1**, (1989) 255.

[7] Sato, T., Hayashi, T., Watanabe, K., Horiuchi, R., Tanaka, M., Sawairi, N., Kusano, K., Phys. Fluids, **B4**, (1992) 450.

Figure Captions

Fig. 1. The simulation model of the tokamak device and its coordinate system.

Fig. 2. Toroidal current distributions against the minor radius at t=0, t=415 τ_{pA}, 447 τ_{pA}, and t=480 τ_{pA}. The magnetic axis corresponds to r = 0.

Fig. 3. Temporal evolutions of the magnetic field energy of n=1 mode and n=2 mode.

Fig. 4. The growth rate of n=1 mode for different S numbers. The solid line, being proportional to $S^{-1/3}$, indicates a theoretical growth rate of the resistive kink mode.

Fig. 5 The evolutions of the equi-contours of the toroidal current (upper panels), the magnetic field lines mapped on a poloidal plane (middle panels), and the equi-contours of the temperature (lower panels) at (a) t=0, (b) t=415 τ_{pA}, (c) t=447 τ_{pA}, and (d) t=480 τ_{pA}.

Fig. 6. Magnetic field lines mapped on a poloidal plane after the toroidal current profile flattening at (a) t=493 τ_{pA}, (b) t=504 τ_{pA}, and (c) t=513 τ_{pA}.

Fig. 7 The evolutions of the equi-contours of the toroidal current (upper panels), the magnetic field lines mapped on a poloidal plane (middle panels), and the equi-contours of the temperature (lower panels) at (a) t=447 τ_{pA}, (b) t=480 τ_{pA}, (c) t=493 τ_{pA}, and (d) t=504 τ_{pA}, when the magnitudes of the n=0 component of all the physical quantities are artificially fixed to those values at t=407 τ_{pA}.

Fig. 8 The evolutions of the equi-contours of the toroidal current (upper panels), the magnetic field lines mapped on a poloidal plane (middle panels), and the equi-contours of the temperature (lower panels) at (a) t=366 τ_{pA}, (b) t=407 τ_{pA}, (c) t=451 τ_{pA}, and (d) t=459 τ_{pA}, when the thermal conductivity effect is removed completely.

Fig. 9 The evolutions of magnetic field lines mapped on a poloidal plane at t=492.9 τ_{pA}, 494.5 τ_{pA}, 496.1 τ_{pA}, 500.2 τ_{pA}, 505.1 τ_{pA}, 505.9 τ_{pA}, 506.7 τ_{pA}, 507.5 τ_{pA}, 508.3

τ_{pA}, and 512.8 τ_{pA}.

Fig. 10 The plasma flow vectors overlayed with the magnetic structure on a poloidal plane at t=505.1 τ_{pA}.

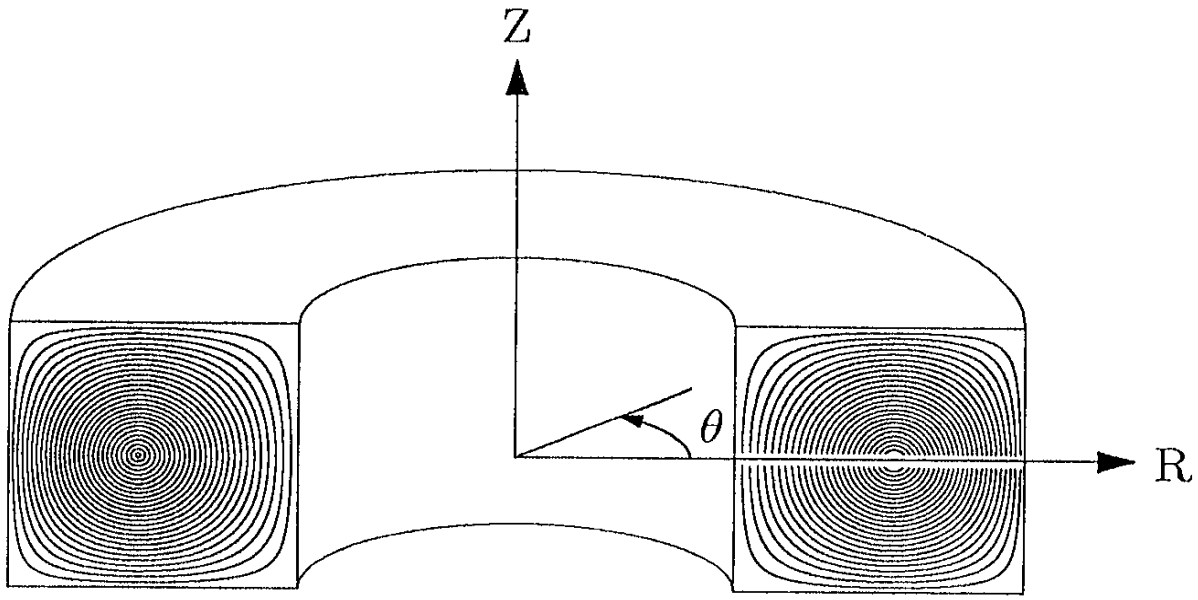

Fig. 1

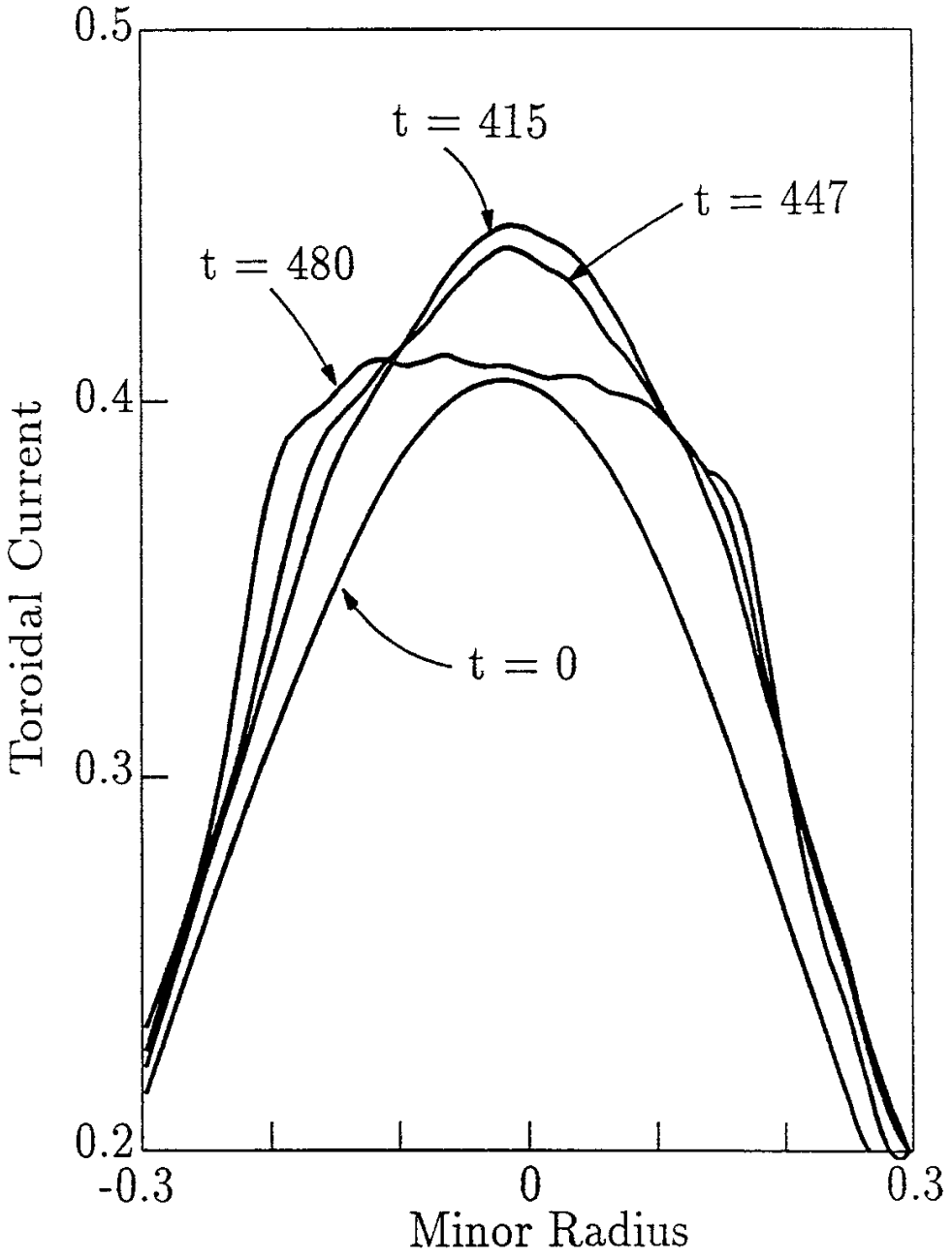
0.5
0.4
0.3
0.2
t = 415
t = 447
t = 480
t = 0
Toroidal Current
-0.3
0
0.3
Minor Radius

Fig. 2

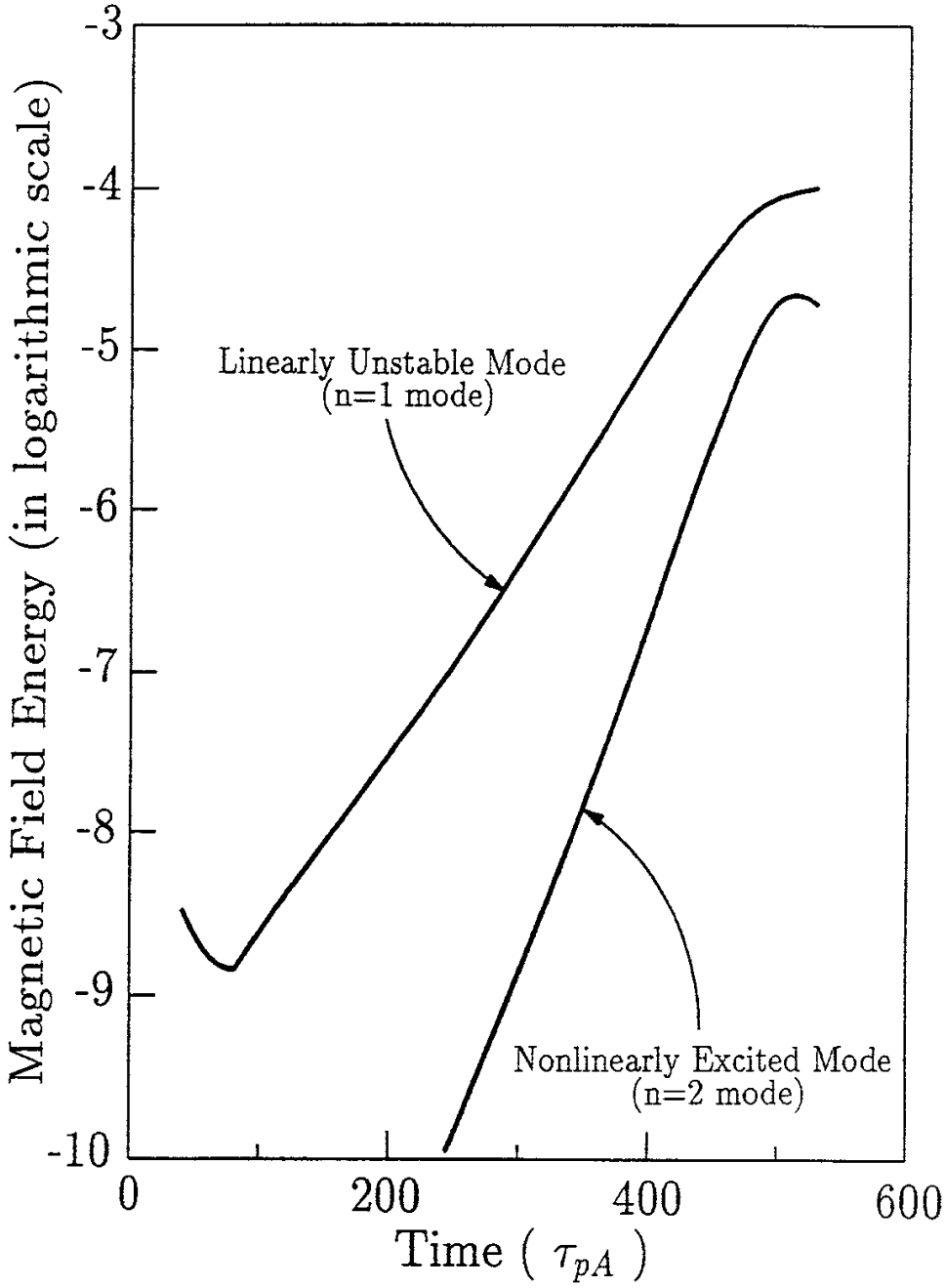
-3
-4
-5
-6
-7
-8
-9
-10
Magnetic Field Energy (in logarithmic scale)
Linearly Unstable Mode
(n=1 mode)
Nonlinearly Excited Mode
(n=2 mode)
0
200
400
600
Time (τ_{pA})

Fig. 3

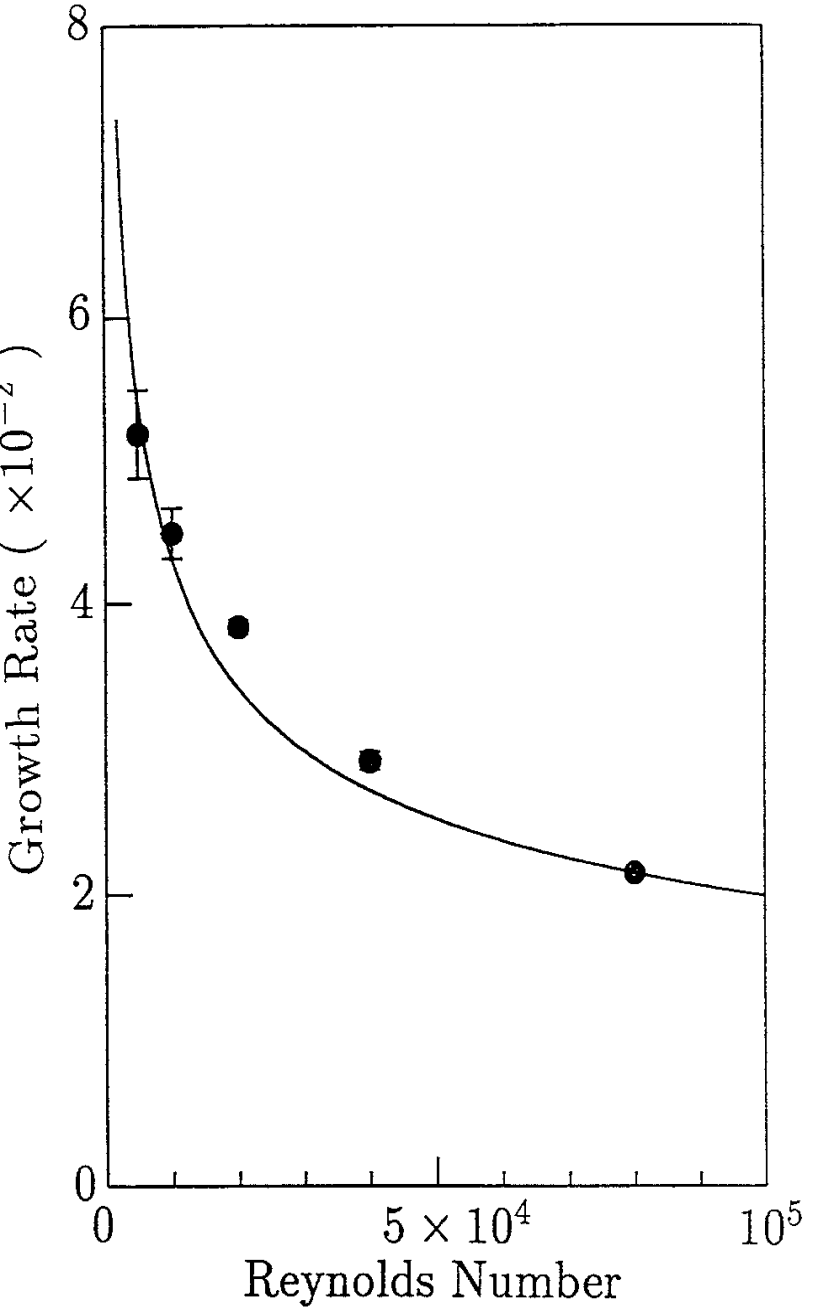
8
6
4
2
0
Growth Rate ($\times 10^{-2}$)
0
5×10^4
10^5
Reynolds Number

Fig. 4

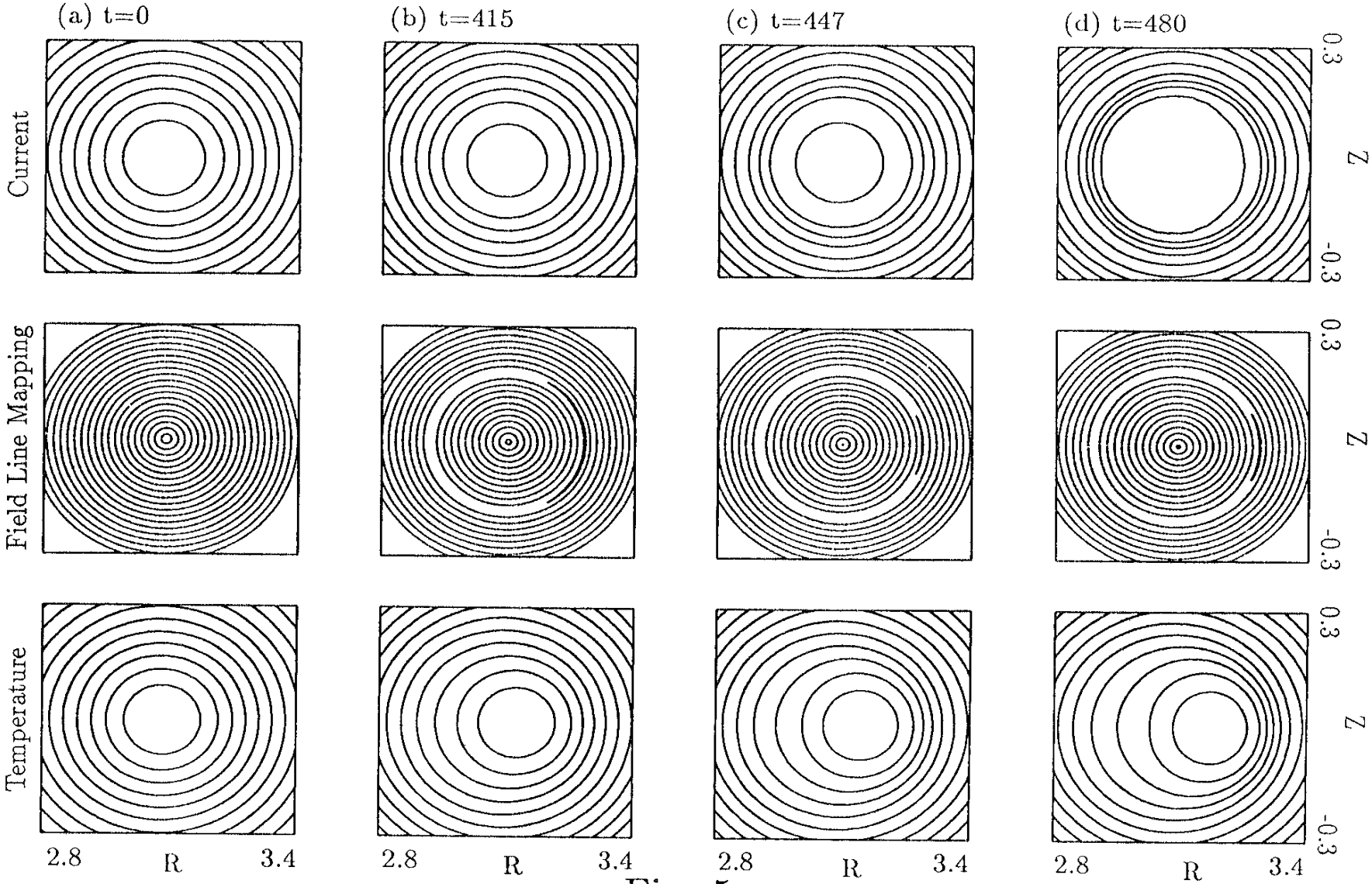
(a) t=0
(b) t=415
(c) t=447
(d) t=480
Current
Field Line Mapping
Temperature
0.3
Z
-0.3
2.8
R
3.4

Fig. 5

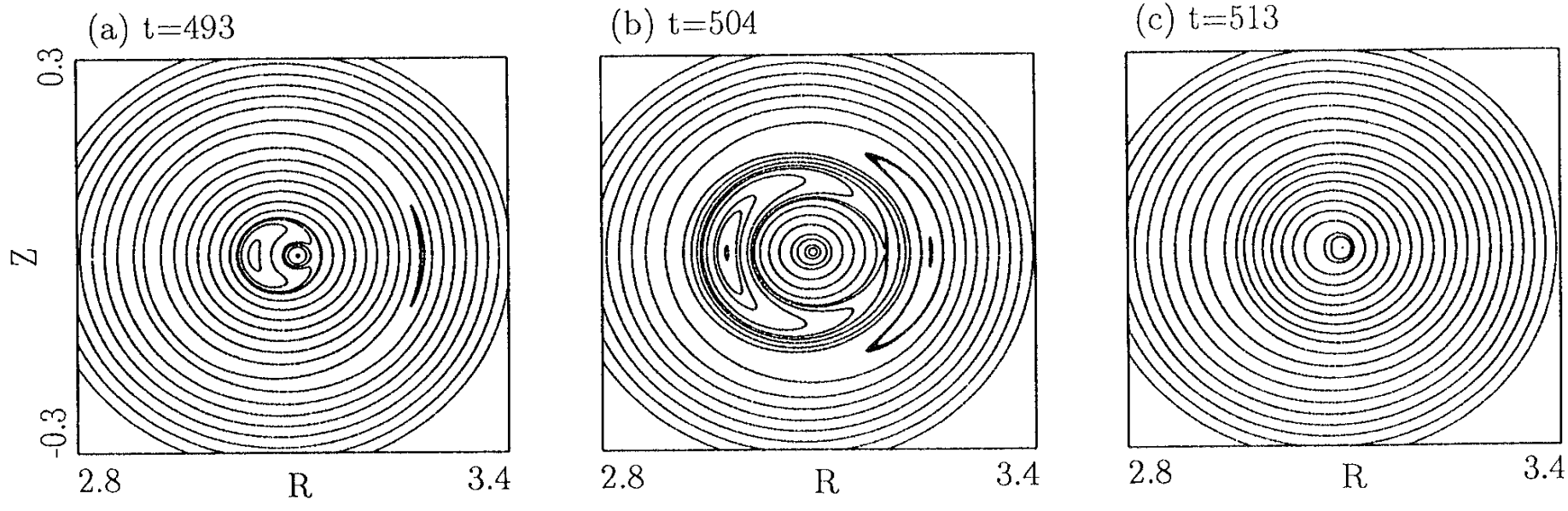

Fig. 6

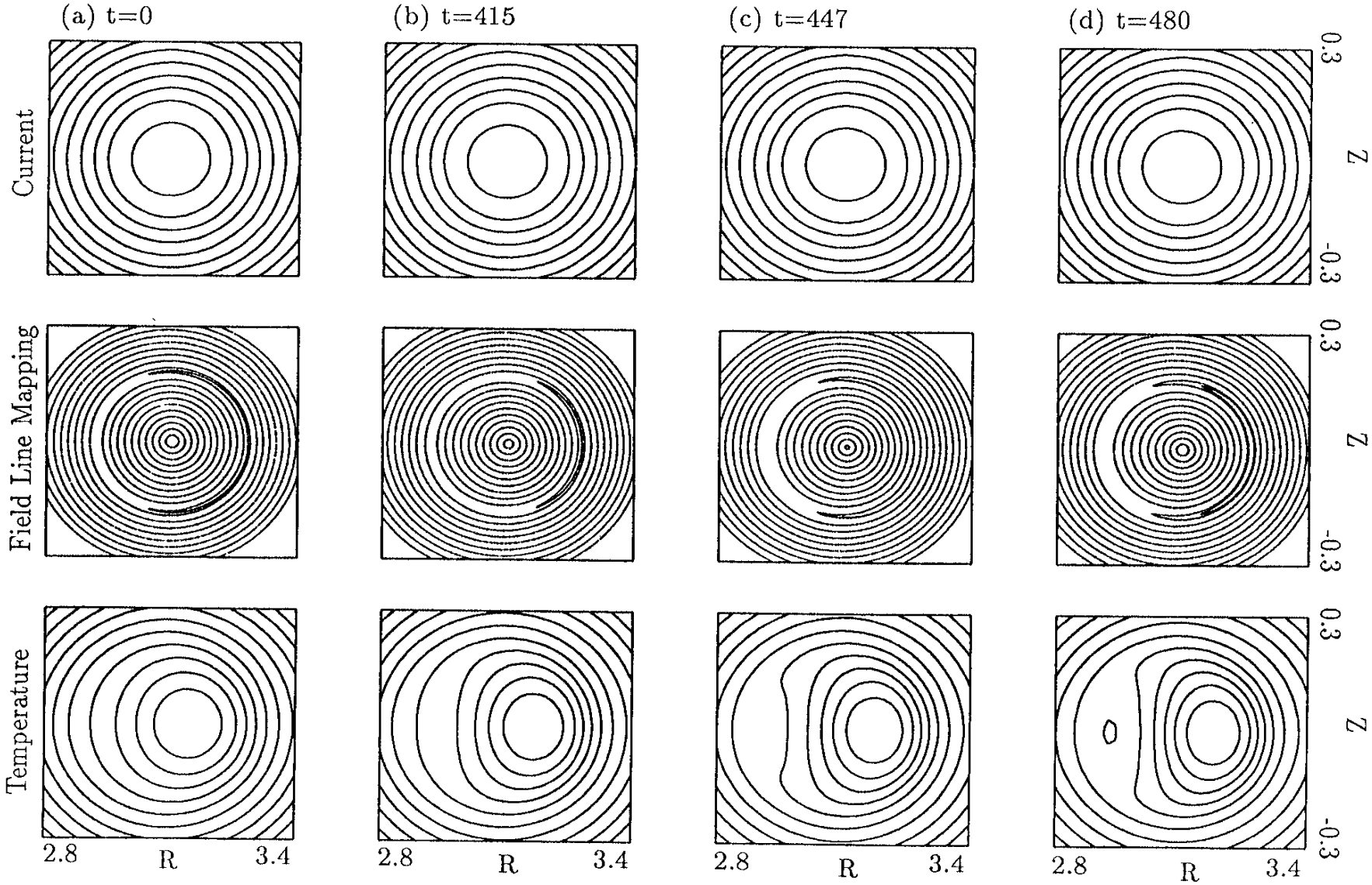
(a) t=0
(b) t=415
(c) t=447
(d) t=480
Current
Field Line Mapping
Temperature
0.3
Z
-0.3
2.8
R
3.4

Fig. 7

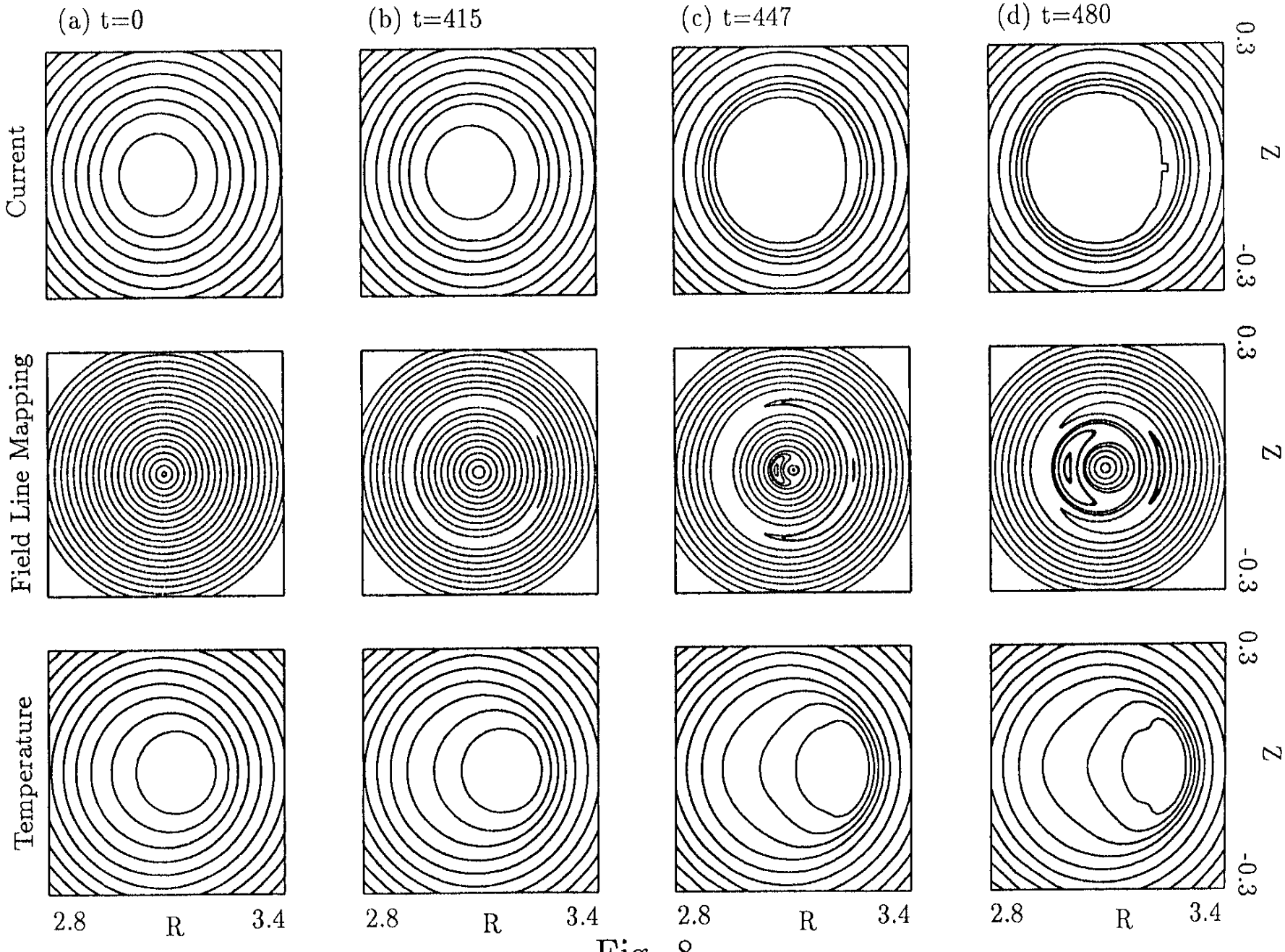
(a) t=0
(b) t=415
(c) t=447
(d) t=480
Current
Field Line Mapping
Temperature
0.3
-0.3
Z
2.8
R
3.4

Fig. 8

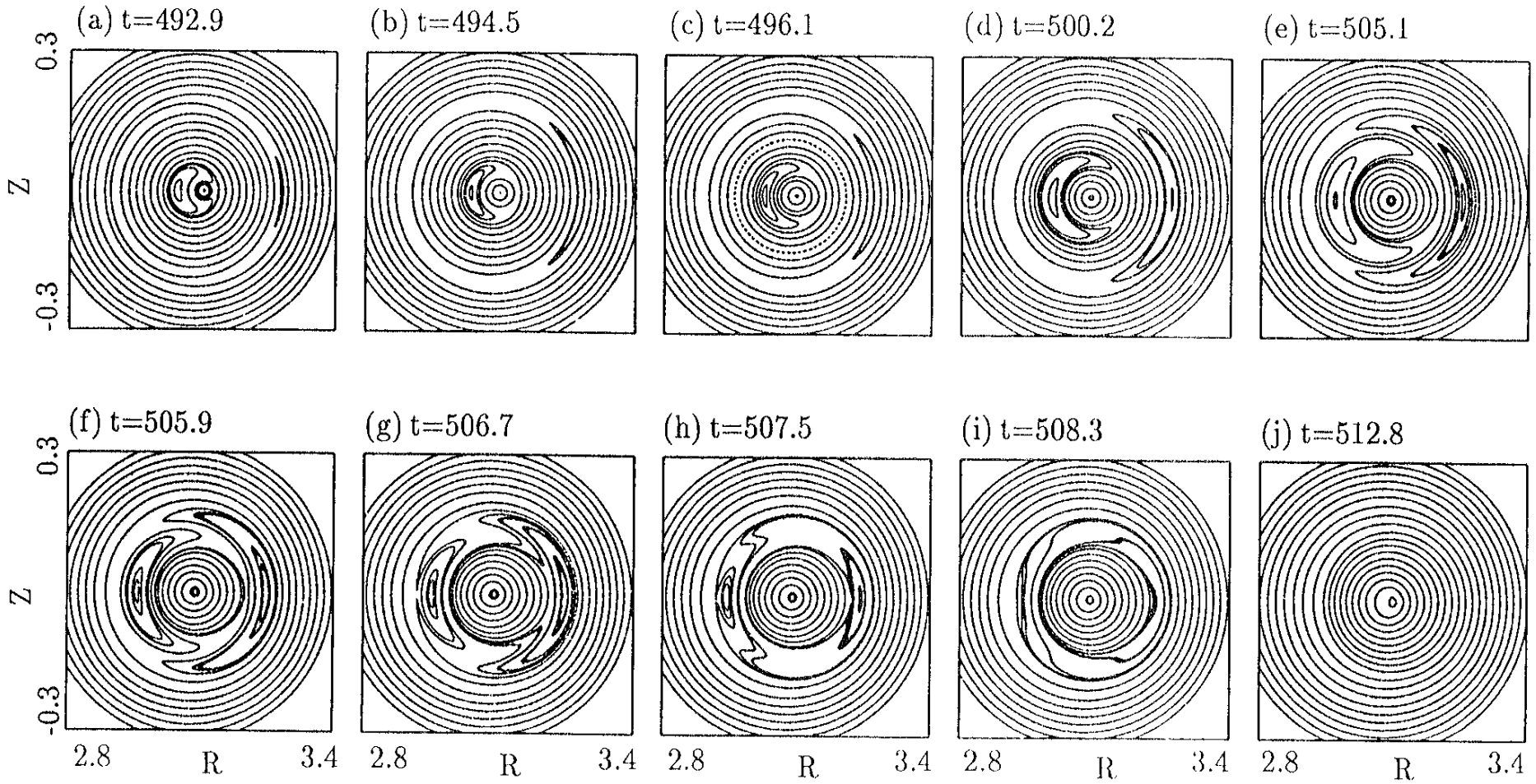
(a) t=492.9
(b) t=494.5
(c) t=496.1
(d) t=500.2
(e) t=505.1
(f) t=505.9
(g) t=506.7
(h) t=507.5
(i) t=508.3
(j) t=512.8
Z
0.3
-0.3
2.8
R
3.4

Fig. 9

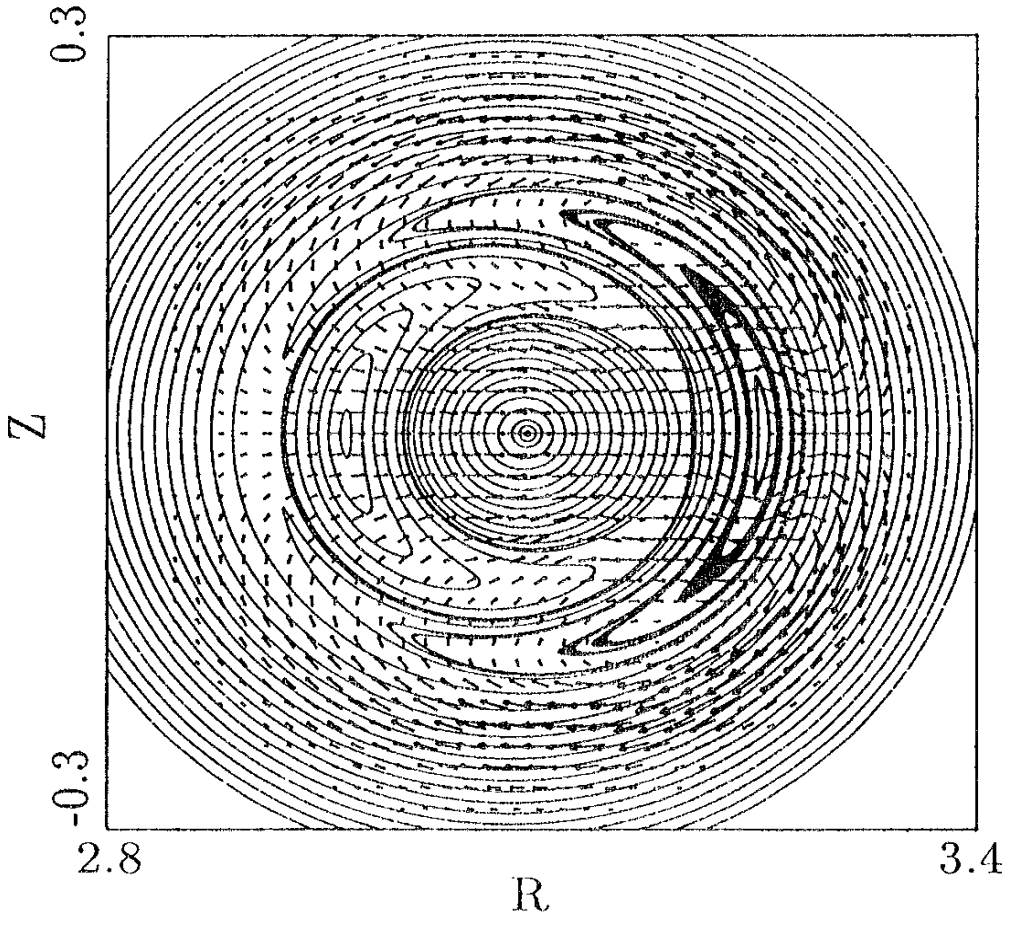

Fig. 10

Recent Issues of NIFS Series

NIFS-273 Y. Hamada, A. Nishizawa, Y. Kawasumi, K. Narihara, K. Sato, T. Seki, K. Toi, H. Iguchi, A. Fujisawa, K. Adachi, A. Ejiri, S. Hidekuma, S. Hirokura, K. Ida, J. Koong, K. Kawahata, M. Kojima, R. Kumazawa, H. Kuramoto, R. Liang, H. Sakakita, M. Sasao, K. N. Sato, T. Tsuzuki, J. Xu, I. Yamada, T. Watari, I. Negi,
Measurement of Profiles of the Space Potential in JIPP T-IIU Tokamak Plasmas by Slow Poloidal and Fast Toroidal Sweeps of a Heavy Ion Beam; Feb. 1994

NIFS-274 M. Tanaka,
A Mechanism of Collisionless Magnetic Reconnection; Mar. 1994

NIFS-275 A. Fukuyama, K. Itoh, S.-I. Itoh, M. Yagi and M. Azumi,
Isotope Effect on Confinement in DT Plasmas; Mar. 1994

NIFS-276 R.V. Reddy, K. Watanabe, T. Sato and T.H. Watanabe,
Impulsive Alfven Coupling between the Magnetosphere and Ionosphere; Apr.1994

NIFS-277 J. Uramoto,
A Possibility of π^- Meson Production by a Low Energy Electron Bunch and Positive Ion Bunch; Apr. 1994

NIFS-278 K. Itoh, S.-I. Itoh, A. Fukuyama, M. Yagi and M. Azumi,
Self-sustained Turbulence and L-mode Confinement in Toroidal Plasmas II; Apr. 1994

NIFS-279 K. Yamazaki and K.Y.Watanabe,
New Modular Heliotron System Compatible with Closed Helical Divertor and Good Plasma Confinement; Apr. 1994

NIFS-280 S. Okamura, K. Matsuoka, K. Nishimura, K. Tsumori, R. Akiyama, S. Sakakibara, H. Yamada, S. Morita, T. Morisaki,. N. Nakajima, K. Tanaka, J. Xu, K. Ida, H. Iguchi, A. Lazaros, T. Ozaki, H. Arimoto, A. Ejiri, M. Fujiwara, H. Idei. O. Kaneko, K. Kawahata, T. Kawamoto, A. Komori, S. Kubo, O. Motojima, V.D. Pustovitov, C. Takahashi, K. Toi and I. Yamada,
High-Beta Discharges with Neutral Beam Injection in CHS; Apr. 1994

NIFS-281 K. Kamada, H. Kinoshita and H. Takahashi,
Anomalous Heat Evolution of Deuteron Implanted Al on Electron Bombardment ; May 1994

NIFS-282 H. Takamaru, T. Sato, K. Watanabe and R. Horiuchi,
Super Ion Acoustic Double Layer; May 1994

NIFS-283 O.Mitarai and S. Sudo
Ignition Characteristics in D-T Helical Reactors; June 1994

NIFS-284 R. Horiuchi and T. Sato,
Particle Simulation Study of Driven Magnetic Reconnection in a Collisionless Plasma; June 1994

NIFS-285 K.Y. Watanabe, N. Nakajima, M. Okamoto, K. Yamazaki, Y. Nakamura, M. Wakatani,
Effect of Collisionality and Radial Electric Field on Bootstrap Current in LHD (Large Helical Device); June 1994

NIFS-286 H. Sanuki, K. Itoh, J. Todoroki, K. Ida, H. Idei, H. Iguchi and H. Yamada,
Theoretical and Experimental Studies on Electric Field and Confinement in Helical Systems; June 1994

NIFS-287 K. Itoh and S-I. Itoh,
Influence of the Wall Material on the H-mode Performance; June 1994

NIFS-288 K. Itoh, A. Fukuyama, S.-I. Itoh, M. Yagi and M. Azumi
Self-Sustained Magnetic Braiding in Toroidal Plasmas: July 1994

NIFS-289 Y. Nejoh,
Relativistic Effects on Large Amplitude Nonlinear Langmuir Waves in a Two-Fluid Plasma; July 1994

NIFS-290 N. Ohyabu, A. Komori, K. Akaishi, N. Inoue, Y. Kubota, A.I. Livshit, N. Noda, A. Sagara, H. Suzuki, T. Watanabe, O. Motojima, M. Fujiwara, A. Iiyoshi,
Innovative Divertor Concepts for LHD; July 1994

NIFS-291 H. Idei, K. Ida, H. Sanuki, S. Kubo, H. Yamada, H. Iguchi, S. Morita, S. Okamura, R. Akiyama, H. Arimoto, K. Matsuoka, K. Nishimura, K. Ohkubo, C. Takahashi, Y. Takita, K. Toi, K. Tsumori and I. Yamada,
Formation of Positive Radial Electric Field by Electron Cyclotron Heating in Compact Helical System; July 1994

NIFS-292 N. Noda, A. Sagara, H. Yamada, Y. Kubota, N. Inoue, K. Akaishi, O. Motojima, K. Iwamoto, M. Hashiba, I. Fujita, T. Hino, T. Yamashina, K. Okazaki, J. Rice, M. Yamage, H. Toyoda and H. Sugai,
Boronization Study for Application to Large Helical Device; July 1994

NIFS-293 Y. Ueda, T. Tanabe, V. Philipps, L. Könen, A. Pospieszczyk, U. Samm, B. Schweer, B. Unterberg, M. Wada, N. Hawkes and N. Noda,
Effects of Impurities Released from High Z Test Limiter on Plasma Performance in TEXTOR; July. 1994

NIFS-294 K. Akaishi, Y. Kubota, K. Ezaki and O. Motojima,

Experimental Study on Scaling Law of Outgassing Rate with A Pumping Parameter, Aug. 1994

NIFS-295 S. Bazdenkov, T. Sato, R. Horiuchi, K. Watanabe
Magnetic Mirror Effect as a Trigger of Collisionless Magnetic Reconnection, Aug. 1994

NIFS-296 K. Itoh, M. Yagi, S.-I. Itoh, A. Fukuyama, H. Sanuki, M. Azumi
Anomalous Transport Theory for Toroidal Helical Plasmas,
Aug. 1994 (IAEA-CN-60/D-III-3)

NIFS-297 J. Yamamoto, O. Motojima, T. Mito, K. Takahata, N. Yanagi, S. Yamada, H. Chikaraishi, S. Imagawa, A. Iwamoto, H. Kaneko, A. Nishimura, S. Satoh, T. Satow, H. Tamura, S. Yamaguchi, K. Yamazaki, M. Fujiwara, A. Iiyoshi and LHD group,
New Evaluation Method of Superconductor Characteristics for Realizing the Large Helical Device; Aug. 1994 (IAEA-CN-60/F-P-3)

NIFS-298 A. Komori, N. Ohyabu, T. Watanabe, H. Suzuki, A. Sagara, N. Noda, K. Akaishi, N. Inoue, Y. Kubota, O Motojima, M. Fujiwara and A. Iiyoshi,
Local Island Divertor Concept for LHD; Aug. 1994 (IAEA-CN-60/F-P-4)

NIFS-299 K. Toi, T. Morisaki, S. Sakakibara, A. Ejiri, H. Yamada, S. Morita, K. Tanaka, N. Nakajima, S. Okamura, H. Iguchi, K. Ida, K. Tsumori, S. Ohdachi, K. Nishimura, K. Matsuoka, J. Xu, I. Yamada, T. Minami, K. Narihara, R. Akiyama, A. Ando, H. Arimoto, A. Fujisawa, M. Fujiwara, H. Idei, O. Kaneko, K. Kawahata, A. Komori, S. Kubo, R. Kumazawa, T. Ozaki, A. Sagara, C. Takahashi, Y. Takita and T. Watari
Impact of Rotational-Transform Profile Control on Plasma Confinement and Stability in CHS; Aug. 1994 (IAEA-CN-60/A6/C-P-3)

NIFS-300 H. Sugama and W. Horton,
Dynamical Model of Pressure-Gradient-Driven Turbulence and Shear Flow Generation in L-H Transition; Aug. 1994 (IAEA/CN-60/D-P-I-11)

NIFS-301 Y. Hamada, A. Nishizawa, Y. Kawasumi, K.N. Sato, H. Sakakita, R. Liang, K. Kawahata, A. Ejiri, K. Narihara, K. Sato, T. Seki, K. Toi, K. Itoh, H. Iguchi, A. Fujisawa, K. Adachi, S. Hidekuma, S. Hirokura, K. Ida, M. Kojima, J. Koog, R. Kumazawa, H. Kuramoto, T. Minami, I. Negi, S. Ohdachi, M. Sasao, T. Tsuzuki, J. Xu, I. Yamada, T. Watari,
Study of Turbulence and Plasma Potential in JIPP T-IIU Tokamak;
Aug. 1994 (IAEA/CN-60/A-2-III-5)

NIFS-302 K. Nishimura, R. Kumazawa, T. Mutoh, T. Watari, T. Seki, A. Ando, S. Masuda, F. Shinpo, S. Murakami, S. Okamura, H. Yamada, K. Matsuoka, S. Morita, T. Ozaki, K. Ida, H. Iguchi, I. Yamada, A. Ejiri, H. Idei, S. Muto, K. Tanaka, J. Xu, R. Akiyama, H. Arimoto, M. Isobe, M. Iwase, O. Kaneko, S. Kubo, T. Kawamoto, A. Lazaros, T. Morisaki, S. Sakakibara, Y. Takita, C. Takahashi and K. Tsumori,

ICRF Heating in CHS; Sep. 1994 (IAEA-CN-60/A-6-I-4)

NIFS-303 S. Okamura, K. Matsuoka, K. Nishimura, K. Tsumori, R. Akiyama, S. Sakakibara, H. Yamada, S. Morita, T. Morisaki, N. Nakajima, K. Tanaka, J. Xu, K. Ida, H. Iguchi, A. Lazaros, T. Ozaki, H. Arimoto, A. Ejiri, M. Fujiwara, H. Idei, A. Iiyoshi, O, Kaneko, K. Kawahata, T. Kawamoto, S. Kubo, T. Kuroda, O. Motojima, V.D. Pustovitov, A. Sagara, C. Takahashi, K. Toi and I. Yamada,
High Beta Experiments in CHS; Sep. 1994 (IAEA-CN-60/A-2-IV-3)

NIFS-304 K. Ida, H. Idei, H. Sanuki, K. Itoh, J. Xu, S. Hidekuma, K. Kondo, A. Sahara, H. Zushi, S.-I. Itoh, A. Fukuyama, K. Adati, R. Akiyama, S. Bessho, A. Ejiri, A. Fujisawa, M. Fujiwara, Y. Hamada, S. Hirokura, H. Iguchi, O. Kaneko, K. Kawahata, Y. Kawasumi, M. Kojima, S. Kubo, H. Kuramoto, A. Lazaros, R. Liang, K. Matsuoka, T. Minami, T. Mizuuchi, T. Morisaki, S. Morita, K. Nagasaki, K. Narihara, K. Nishimura, A. Nishizawa, T. Obiki, H. Okada, S. Okamura, T. Ozaki, S. Sakakibara, H. Sakakita, A. Sagara, F. Sano, M. Sasao, K. Sato, K.N. Sato, T. Saeki, S. Sudo, C. Takahashi, K. Tanaka, K. Tsumori, H.Yamada, I. Yamada, Y. Takita, T. Tuzuki, K. Toi and T. Watari,
Control of Radial Electric Field in Torus Plasma; Sep. 1994
(IAEA-CN-60/A-2-IV-2)

NIFS-305 T. Hayashi, T. Sato, N. Nakajima, K. Ichiguchi, P. Merkel, J. Nührenberg, U. Schwenn, H. Gardner, A. Bhattacharjee and C.C.Hegna,
Behavior of Magnetic Islands in 3D MHD Equilibria of Helical Devices;
Sep. 1994 (IAEA-CN-60/D-2-II-4)

NIFS-306 S. Murakami, M. Okamoto, N. Nakajima, K.Y. Watanabe, T. Watari, T. Mutoh, R. Kumazawa and T. Seki,
Monte Carlo Simulation for ICRF Heating in Heliotron/Torsatrons;
Sep. 1994 (IAEA-CN-60/D-P-I-14)

NIFS-307 Y. Takeiri, A. Ando, O. Kaneko, Y. Oka, K. Tsumori, R. Akiyama, E. Asano, T. Kawamoto, T. Kuroda, M. Tanaka and H. Kawakami
Development of an Intense Negative Hydrogen Ion Source with a Wide-Range of External Magnetic Filter Field; Sep. 1994

NIFS-308 T. Hayashi, T. Sato, H.J. Gardner and J.D. Meiss,
Evolution of Magnetic Islands in a Heliac; Sep. 1994

NIFS-309 H. Amo, T. Sato and A. Kageyama,
Intermittent Energy Bursts and Recurrent Topological Change of a Twisting Magnetic Flux Tube; Sep.1994

NIFS-310 T. Yamagishi and H. Sanuki,
Effect of Anomalous Plasma Transport on Radial Electric Field in Torsatron/Heliotron; Sep. 1994